

This document is confidential and is proprietary to the American Chemical Society and its authors. Do not copy or disclose without written permission. If you have received this item in error, notify the sender and delete all copies.

Phosphorene and Black Phosphorus: the ^{31}P NMR View

Journal:	<i>The Journal of Physical Chemistry Letters</i>
Manuscript ID	jz-2019-01788z
Manuscript Type:	Letter
Date Submitted by the Author:	20-Jun-2019
Complete List of Authors:	<p>Martini, Francesca; Universita degli Studi di Pisa Facolta di Scienze Matematiche Fisiche Naturali, Chimica e Chimica Industriale</p> <p>Borsacchi, Silvia; Consiglio Nazionale delle Ricerche – CNR, Istituto di Chimica dei Composti OrganoMetallici</p> <p>Barcaro, Giovanni; Consiglio Nazionale delle Ricerche, Istituto per i Processi Chimico-Fisici</p> <p>Caporali, Maria; Istituto di Chimica dei Composti Organo Metallici Consiglio Nazionale delle Ricerche,</p> <p>Vanni, Matteo; ICCOM CNR Firenze,</p> <p>Serrano-Ruiz, Manuel; Istituto di Chimica dei Composti Organo Metallici Consiglio Nazionale delle Ricerche,</p> <p>Geppi, Marco; Universita degli Studi di Pisa, Dipartimento di Chimica e Chimica Industriale</p> <p>Peruzzini, Maurizio; Istituto di Chimica dei Composti Organo Metallici Consiglio Nazionale delle Ricerche,</p> <p>Calucci, Lucia; Consiglio Nazionale delle Ricerche, Istituto di Chimica dei Composti OrganoMetallici</p>

SCHOLARONE™
Manuscripts

Phosphorene and Black Phosphorus: the ^{31}P NMR View

Francesca Martini,^{1,2} Silvia Borsacchi,^{2} Giovanni Barcaro,³ Maria Caporali,⁴ Matteo Vanni,^{4,5}*

Manuel Serrano-Ruiz,⁴ Marco Geppi,^{1,2} Maurizio Peruzzini,⁴ Lucia Calucci²

1. Department of Chemistry and Industrial Chemistry, University of Pisa, via G.

Moruzzi 13, I-56124 Pisa, Italy

2. Institute for the Chemistry of OrganoMetallic Compounds, Italian National Council

for Research, CNR-ICCOM, via G. Moruzzi 1, I-56124 Pisa, Italy

3. Institute for the Physico-Chemical Processes, Italian National Council for Research,

CNR-IPCF, via G. Moruzzi 1, I-56124 Pisa, Italy.

4. Institute for the Chemistry of OrganoMetallic Compounds, Italian National Council

for Research, CNR-ICCOM, Via Madonna del Piano 10, I-50019 Sesto Fiorentino, Italy

5. Department of Biotechnology, Chemistry and Pharmacy, University of Siena, via

Aldo Moro 2, I-53100 Siena, Italy

AUTHOR INFORMATION

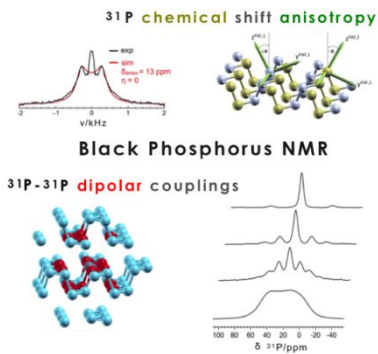
Corresponding Author

*silvia.borsacchi@cnr.it

ABSTRACT.

This work aims at characterizing for the first time the ^{31}P spin interactions determining the Nuclear Magnetic Resonance (NMR) properties of solid black phosphorus (bP) and of its few-layer exfoliated (fl-bP) form. Indeed, the knowledge of these properties is still very poor, in spite of the great interest received by this layered phosphorus allotrope and its exfoliated 2D form, phosphorene. By combining Density Functional Theory (DFT) calculations and Solid State NMR experiments on suspensions of fl-bP nanoflakes and on solid black phosphorus, it has been possible to characterize the ^{31}P homonuclear dipolar and chemical shift interactions, identifying the network of ^{31}P nuclei more strongly dipolarly coupled and highlighting two kinds of magnetically non-equivalent ^{31}P nuclei. These results add an important missing piece of information to the fundamental chemico-physical knowledge of bP and support future extensive applications of NMR spectroscopy to the characterization of phosphorene-based materials.

TOC GRAPHICS



KEYWORDS. 2D materials, DFT, chemical shielding anisotropy, homonuclear dipolar coupling, ³¹P MAS.

The isolation of graphene in 2004¹ opened the way to the new fascinating world of 2D materials: from bi-dimensionality peculiar physical and chemical properties can arise, which make 2D materials extremely attractive for many different application fields, including electronics, photonics, spintronics, mechanics and medicine. In this scenario black phosphorus (bP), the most stable allotrope of elemental phosphorus, attracted in the last few years a great interest. Indeed, it is characterized by a layered crystal structure (Figure 1), in which the inter-layer bonding energy is sufficiently low to allow exfoliation by several methods.² In every layer, each phosphorus atom covalently bonds with three phosphorus atoms and bears a lone pair.^{3,4} Thus the atomic structure of the single layer of bP, commonly named phosphorene, is not planar and a zig-zag and an armchair directions can be distinguished. From these structural features an in-plane anisotropy arises, which affects the chemico-physical properties and opens the field to important electronic and optical applications. Moreover bP has a direct and tunable band gap that goes from 0.3 eV in the bulk to 2 eV in the monolayer, thus covering a range between graphene and transition metal dichalcogenides, which makes it highly attractive as 2D semi-conductor.^{5,6,7,8,9} Many efforts have been devoted also to study the surface functionalization of phosphorene, aiming to widen its applications and to protect it against ambient degradation.^{5,6,10,11} Indeed phosphorene is prone to oxidation, which represents a serious practical limitation to its use. Recently important biomedical applications of exfoliated bP have also been reported.¹²

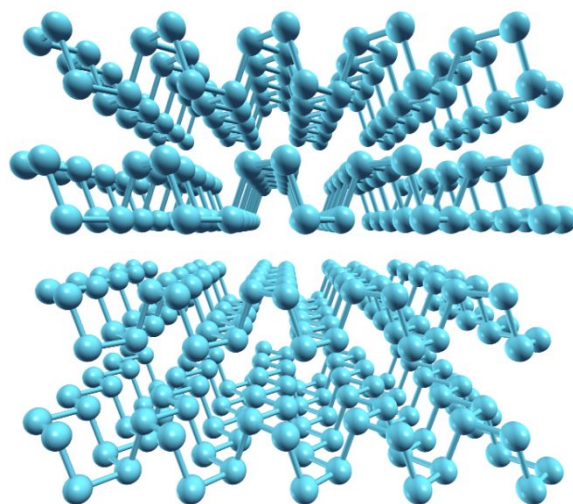


Figure 1. Layered crystal structure of bP.

An accurate structural control of this material is clearly crucial and, to this aim, Nuclear Magnetic Resonance (NMR) spectroscopy is one of the most powerful techniques for shedding light onto chemical structural features. On the other hand, when exfoliated bP is dispersed in a solvent, commonly as few-layer bP (fl-bP), the relatively large size of the obtainable nanoflakes (lateral dimension of 100-400 nm and thickness of 10-50 nm) and their slow and anisotropic tumbling motions, make fl-bP undetectable with standard solution-state NMR techniques.¹³ We published the first ³¹P Magic Angle Spinning (MAS) NMR spectrum of fl-bP embedded in polymeric matrices:⁹ the use of solid state NMR techniques allowed the easy observation of the signals of embedded fl-bP and of its oxidized species. Moreover, the variation of the degree of oxidation with

the preparation method was highlighted. Very recently the use of MAS also allowed us to record the first ^{31}P NMR spectrum of fl-bP directly in solvent suspension, which was used for inspecting its possible functionalization with boronic acid derivatives.¹¹

In spite of the great interest paid in these years to phosphorene, a thorough report and comprehension of the fundamental ^{31}P NMR properties of its best analogous fl-bP is not present in the literature. Also for bP, even if the application of Solid State NMR is rapidly increasing, only a few works are present in the literature, mainly reporting the bP isotropic signal and/or the signals of some degradation or functionalization products^{14,15,16,17,18,19,20,21}, with only one work proposing a qualitative interpretation of the static ^{31}P spectrum.²² Thus, the aim of the present work is to identify and quantify the ^{31}P nuclear spin interactions determining the NMR properties of fl-bP and bP, not only for adding a missing piece to the physico-chemical knowledge of bP, but also because NMR can add a great value to the future characterization of innovative phosphorene-based materials. We started from the analysis of ^{31}P MAS NMR spectra of samples of fl-BP with different nanoflake size, suspended in different solvents (samples preparation is reported in the Supporting Information). Then, once assessed the similarity of these spectra with those of crystalline bP, a thorough analysis of the ^{31}P spin interactions was carried out on bP by combining Solid State NMR techniques and DFT calculations.

Figures 2a and 2b show the ^{31}P static and MAS NMR spectra of tetrahydrofuran suspensions of large fl-bP nanoflakes with an average lateral dimension of 400-700 nm (Figure S1) and a thickness of 10-50 nm (Figure S2). As already reported,¹¹ the use of MAS allows the broad static signal of fl-bP to be partially resolved in a signal at the isotropic chemical shift of 18.5 ± 0.5 ppm, identified by recording spectra at different MAS frequencies (in the range 0.5-3 kHz, not shown), and a series of spinning sidebands, which arise from the anisotropic nuclear spin interactions of ^{31}P nuclei, i.e., in principle, chemical shielding and homonuclear dipolar interactions. The degree of spectral resolution obtainable at a MAS frequency of 3 kHz and the isotropic peak of fl-bP observed are similar for a suspension of smaller fl-bP nanoflakes (Figure 2c), having an average lateral dimension of 100-400 nm and a thickness less than 15 nm (Figures S3 and S4, respectively). On the other hand, in the spectrum of the sample constituted by smaller nanoflakes (Figure 2c) signals at about $1 \div 2$ ppm and -20 ppm are evident, even if superimposed to spinning sidebands, which can be ascribed to products of the oxidative degradation of fl-bP, likely favoured by the smaller size and thickness of the nanoflakes. From the analysis of the ^{31}P spectra recorded with and without ^1H high-power decoupling (Figure S5), it was possible to assign the observed peaks to cyclic trimethaphosphate ($\delta = -20$ ppm), variously protonated phosphate (PO_4^{3-}) ($\delta = 1.33, 1.89$ and 2.50 ppm) and phosphite (HPO_3^{2-}) anions ($\delta = 2.95$ ppm).^{13-16,23}

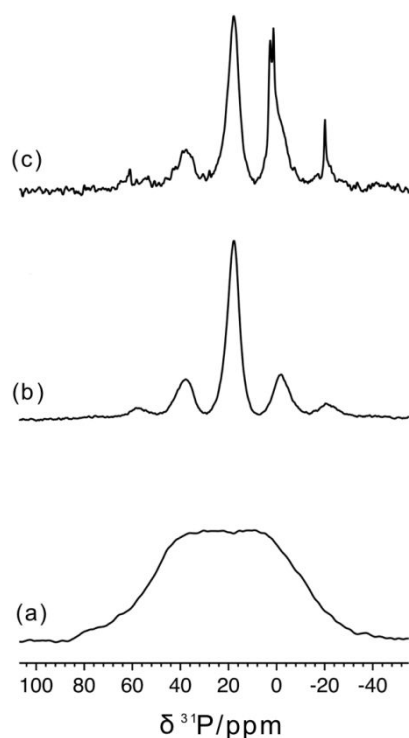


Figure 2. ^{31}P NMR spectra of: large fl-bP nanoflakes suspended in tetrahydrofuran under (a) static and (b) MAS (3 kHz) conditions; (c) small fl-bP nanoflakes suspended in tetrahydrofuran under MAS conditions (3 kHz).

^{31}P MAS spectra of fl-bP suspensions in dimethyl sulfoxide and methanol were also recorded, with the aim of highlighting possible effects of the solvent on ^{31}P chemical shift, in analogy to what observed for molecular phosphorus compounds, such as phosphines and phosphates. The three chosen organic solvents have a different dielectric constant ($\epsilon = 7.58, 32.7$ and 46.7 for tetrahydrofuran, methanol and dimethyl sulfoxide, respectively) and may show a different solvation effect and hydrogen-bond donating ability. As evident in Figure S6, no significant solvent effects were observed

from the spectra. This result, together with the substantial similarity of the ^{31}P spectra of suspensions of larger and smaller fl-bP nanoflakes, indicates that possible edge effects are negligible. Moreover, it is evident that the possible differences in the tumbling motions of nanoflakes with different size do not substantially affect the NMR spectra (Figure 2b and 2c), likely being much slower than the static linewidth. Accordingly, the ^{31}P spin-lattice relaxation time (T_1) of fl-bP measured in suspension was found to be 16 ± 1 s. The scarce effects of nanoflakes tumbling on ^{31}P NMR spectra in suspension are further confirmed by the observed similarity between the static and MAS spectra of the suspensions (Figure 2) and the corresponding spectra of solid bP (Figure 3a).

On the basis of these results it is possible to infer that the extent of the main nuclear spin interactions (homonuclear dipolar coupling and chemical shielding) determining the ^{31}P spectra of solid bP and fl-bP in suspension are substantially the same. The possibility of working on a solid sample increases both the sensitivity and, thanks to the exploitation of higher MAS frequencies (not achievable with samples suspended in a solvent), the spectral resolution. In Figure 3a the static and MAS spectra of bP recorded with MAS frequency up to 16 kHz are reported; all the spectra were recorded taking into account the measured value of ^{31}P T_1 of 40 s. For MAS frequencies up to 1 kHz the spectrum (not shown) is substantially superimposable to the static one, while at 2 kHz a separation in a central isotropic signal and spinning sidebands (placed at multiples of the MAS frequency with respect to the central peak) becomes visible. With increasing

the MAS frequency all peaks progressively narrow, the separation between the isotropic peak and the spinning sidebands increases and the intensity of the sidebands decreases. This behavior, revealing a certain inhomogeneous character of the spin interactions at relatively high MAS frequency, was observed and deeply analyzed by Spiess and co-workers for ^1H homonuclear dipolar-coupled multi-spin systems in organic solids.^{24,25} At 16 kHz the spinning sidebands substantially disappear and only the isotropic peak at 20.5 ± 0.5 ppm is observed. It is worth to notice that, as already reported,⁹ the lineshape is slightly asymmetric and a deconvolution procedure can reveal the presence of a minor signal at slightly higher chemical shift (≈ 23 ppm), which can be tentatively ascribed to a small fraction of slightly structurally different bP.

In giving the theoretical framework to analyze the spectral evolution of homonuclear dipolar-coupled spin systems under MAS, Spiess and coauthors²⁴ demonstrated that in the “fast spinning regime” the integral intensities of the central line and of the first order sidebands are mainly determined by two-spin contributions to the dipolar interactions, while contributions from the correlation of three or more spins can be safely neglected. In particular, the signal intensities I_n of the different peaks can be theoretically obtained as a function of the MAS frequency ω_R as:

$$I_n \approx I(0) \left[\delta_{n,0} + \sum_{i,j}^N \frac{A_n}{\omega_R^2} \left(\omega_D^{ij} \right)^2 \right] \quad (1)$$

where $\delta_{n,0}$ is the Kronecker delta, n is the sideband order, $I(0)$ is the overall integral signal intensity, $\omega_D^{ij} = \frac{\mu_0}{4\pi} \frac{\gamma^2 \hbar}{r_{ij}^3}$ is the dipolar coupling frequency of a given i,j spin pair, $A_0 = -0.3375$, and $A_1 = 0.1524$. In Figure 3b theoretical and experimental values of the intensity of the central line (I_0) and of the first-order sideband (I_1) have been plotted as a function of $(\omega_D^{eff}/\omega_R)^2$, where:

$$\omega_D^{eff} = \sqrt{\sum_{ij}^N (\omega_D^{ij})^2} \quad (2)$$

is an effective dipolar coupling. Different cases have been considered by running the sums in equations (1) and (2) on a different number of pairs of ^{31}P nuclei. In particular, the pairs considered in the sums were those between a chosen ^{31}P nucleus and all the ^{31}P nuclei within a given distance (*threshold*) from it (taken from the optimized bP crystal structure, *vide infra*). In Figure 3b, three cases have been reported, with threshold values of 2.30, 3.55, and 4.00 Å, corresponding to $\omega_D^{eff}/2\pi$ values of 3016.5, 3318.9, 3410.2 Hz, respectively. In particular, only the 3 ^{31}P nuclei closest to the chosen P (all belonging to the same layer) are considered in the first case, while the threshold of 3.55 Å includes the 11 closest ^{31}P nuclei of the same layer. At last, increasing the threshold up to 4 Å also the couplings with the closest 4 ^{31}P nuclei in the adjacent layer are considered. The ^{31}P nuclei considered in the three calculations are highlighted in Figure 3c. It is possible to observe that the experimental trends are very well reproduced in the

1
2
3 last case (threshold = 4 Å): this demonstrates that the homonuclear ^{31}P - ^{31}P dipolar
4
5
6 interactions determining the MAS NMR spectra of bP are those of one P nucleus with
7
8
9 its 15 closest crystallographic neighbors, 11 in the same layer and 4 in the adjacent layer.
10
11 By further extending the set of ^{31}P nuclei considered in the calculation, we could
12
13
14 observe that the sum of the squared residues and the value of ω_D^{eff} reach an horizontal
15
16
17 asymptote for slightly higher threshold values (see Figure S7). It is worth noticing that
18
19
20 this is the first time that the method proposed by Spiess²⁴ for correlating the extent of
21
22
23 the ^1H - ^1H homonuclear dipolar interaction to the structural features of an organic solid
24
25
26 has been applied to ^{31}P nuclei in an inorganic material.
27
28
29
30
31
32
33
34
35
36
37
38
39
40
41
42
43
44
45
46
47
48
49
50
51
52
53
54
55
56
57
58
59
60

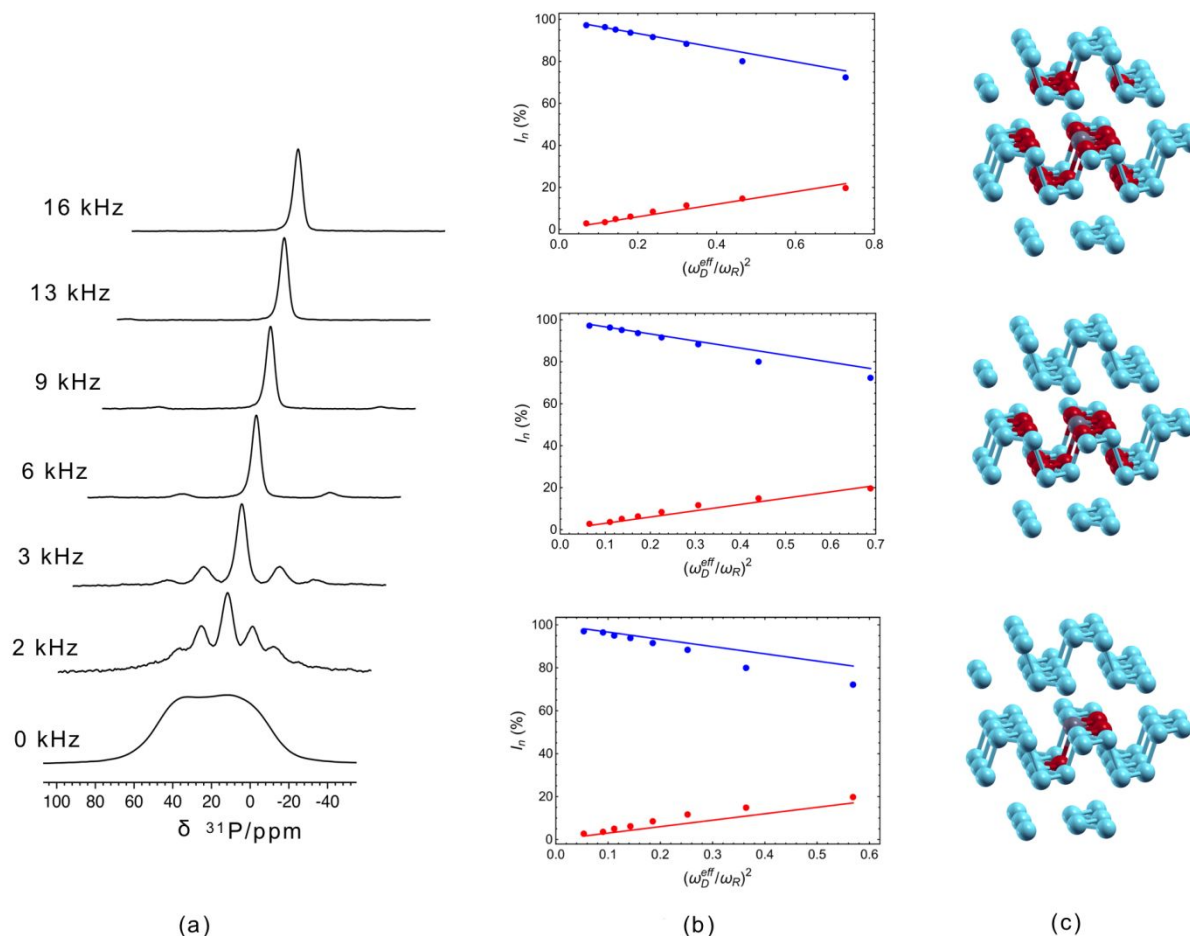


Figure 3. (a) ^{31}P NMR spectra of bP recorded under static (0 kHz) and MAS (from bottom to top at a frequency of 2, 3, 6, 9, 13, 16 kHz) conditions; (b-c) trends of the experimental integral intensities of the isotropic peak (blue circles) and of the first order sidebands (red circles) as a function of $(\omega_D^{\text{eff}}/\omega_R)^2$. The blue and red lines represent the corresponding theoretical values calculated following equations 1 and 2. The three graphs have been obtained including in the calculation of ω_D^{eff} and of the theoretical intensities the dipolar couplings of a given ^{31}P nucleus (coloured in grey in c) with the ^{31}P nuclei within a distance of 2.30, 3.55, and 4.00 Å (coloured in red in c); 3, 11, and 15 pairs of nuclei were included in the calculations in the three cases, respectively.

Once established the strength of the effective dipolar coupling, it is interesting to characterize the chemical shielding interaction of ^{31}P nuclei in bP. This has been done by exploiting an anisotropic – isotropic correlation experiment based on the symmetry sequence R10_1^3 .^{26,27} In particular, the sequence R10_1^3 selectively recouples the second-rank spatial component of the chemical shielding tensor, while completely suppressing the homonuclear dipole-dipole interaction.²⁸ In Figure 4 the 2D ^{31}P anisotropic – isotropic chemical shift correlation spectrum of bP is shown together with the experimental and simulated ^{31}P line shapes obtained for the ^{31}P isotropic peak at 20 ppm. From the simulation it has been possible to determine a chemical shift anisotropy $\delta_{\text{aniso}} = 13$ ppm and an asymmetry $\eta = 0$ (defined following the Haeberlen-Mehring-Spiess convention²⁹), corresponding to the following values of the chemical shift tensor components in its principal axis frame (PAF) $\delta_{zz}^{\text{PAF}} = 29$ ppm, $\delta_{xx}^{\text{PAF}} = \delta_{yy}^{\text{PAF}} = 16$ ppm. It can be noticed that the chemical shift anisotropy, at the ^{31}P Larmor frequency of the experiments, is about 2100 Hz, thus smaller than the effective main ^{31}P - ^{31}P homonuclear dipolar interaction (about 3400 Hz).

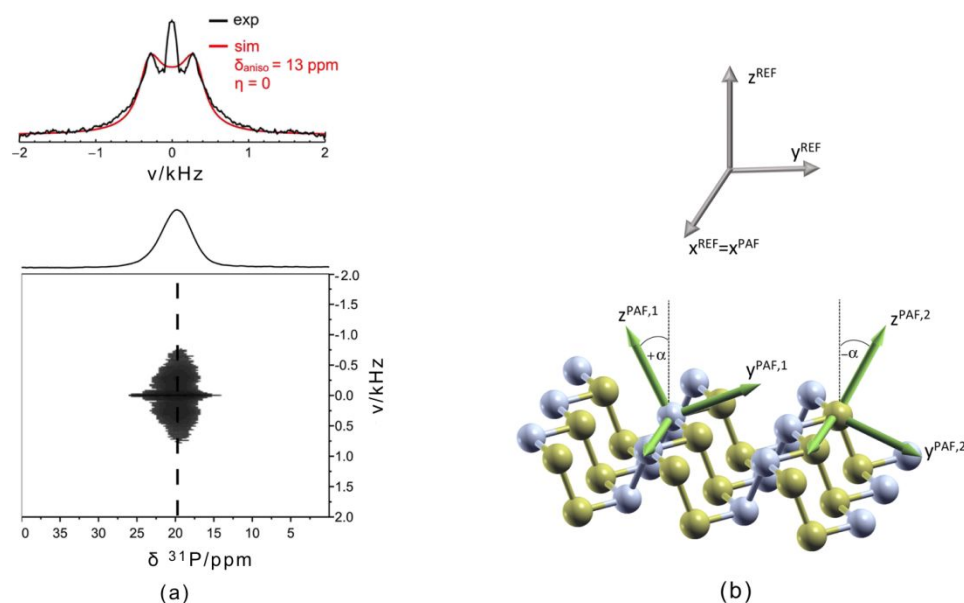


Figure 4. (a) 2D ^{31}P anisotropic – isotropic correlation spectrum of bP obtained by the symmetry sequence R10₁³ and, on the top, experimental (black line) and simulated (red line) ^{31}P CSA line shapes corresponding to the ^{31}P isotropic peak at 20 ppm. The values of chemical shift anisotropy, δ_{aniso} and asymmetry, η , used in the simulation are reported in the figure. δ_{aniso} and η are defined according to the Haeberlen-Mehring-Spiess convention as $\delta_{\text{aniso}} = \delta_{\text{zz}}^{\text{PAF}} - (\delta_{\text{xx}}^{\text{PAF}} + \delta_{\text{yy}}^{\text{PAF}})/2$ and $\eta = (\delta_{\text{yy}}^{\text{PAF}} - \delta_{\text{xx}}^{\text{PAF}})/(\delta_{\text{zz}}^{\text{PAF}} - \delta_{\text{iso}})$ where $|\delta_{\text{zz}}^{\text{PAF}} - \delta_{\text{iso}}| \geq |\delta_{\text{xx}}^{\text{PAF}} - \delta_{\text{iso}}| \geq |\delta_{\text{yy}}^{\text{PAF}} - \delta_{\text{iso}}|$ and $\delta_{\text{iso}} = (\delta_{\text{xx}}^{\text{PAF}} + \delta_{\text{yy}}^{\text{PAF}} + \delta_{\text{zz}}^{\text{PAF}})/3$.

Thus, in order to fully characterize the ^{31}P spin interactions in bP, we also determined the orientation of the ^{31}P chemical shift tensors by Density Functional Theory calculations (computational details are reported in the Supporting Information).^{30,31} The optimized cell parameters correspond to a tetragonal box with sides $3.33 \times 4.42 \times 10.48$ Å (in very good agreement with the experimental values $3.31 \times 4.38 \times 10.48$ Å). Within the unit cell, the structure of bP is determined by using 8 atoms, organized in two separate layers (4 P atoms per layer) held together by weaker (dispersive) interactions.

Focusing on the structure of the single layer (shown in Figure 4b), as already mentioned, each P atom is surrounded by three first-neighbors, at a distance of 2.23-2.26 Å; the atoms are organized according to an armchair configuration and can be grouped in stripes at two different heights. According to the results of the simulation, the 4 atoms of the layer are not magnetically equivalent, but can be divided in two groups (coloured in grey and yellow in Figure 4b), having the same principal values of the chemical shift tensors but a different orientation of their principal axes frames ($x^{\text{PAF},i}$, $y^{\text{PAF},i}$, $z^{\text{PAF},i}$, with $i = 1, 2$) with respect to a common reference frame (x^{REF} , y^{REF} , z^{REF}) in which the x^{REF} axis is aligned along the stripe direction (Figure 4b). The principal axes frames of the chemical shift tensors of the two magnetically inequivalent phosphorus nuclei have the $x^{\text{PAF},i}$ axes coincident with x^{REF} , while the $y^{\text{PAF},i}$ and $z^{\text{PAF},i}$ axes can be obtained from y^{REF} and z^{REF} by a rotation of $+\alpha$ or $-\alpha$ about x^{REF} , with $\alpha \approx 26^\circ$. By considering the experimental values previously determined for the principal components of the chemical shift tensor, it can be observed that the most shielded axis $z^{\text{PAF},i}$ is approximately aligned with the P lone pair.

The isotropic chemical shift of bP is predicted by DFT to be 49 ppm. Although this value is quite different from the experimental one (about 20 ppm), it can be considered satisfactory taking into account the wide range of shifts characterizing P atoms in different chemical environments,³² and the inherent difficulties in achieving a full reproduction of the experimental values in each chemical environment. In addition to

the isotropic shift, DFT also predicts that each atom is characterized by an anisotropy of 25 ppm and η of 0.06-0.07, in good agreement with the experimental results.

In conclusion, by exploiting Solid State NMR techniques we could record and analyze ^{31}P NMR spectra of fl-bP nanoflakes suspended in solvent, observing negligible effects of both the size of the nanoflakes and the nature of the solvent and identifying the main oxidized species formed. The main nuclear spin interactions occurring in solid bP, substantially similar to those of its exfoliated form fl-bP, were characterized by combining Solid State NMR experiments and DFT calculations. It emerged that a prominent role is played by the ^{31}P - ^{31}P homonuclear dipolar interaction, which, by applying for the first time to ^{31}P nuclei in an inorganic material a method proposed for ^1H nuclei in organic solids,²⁴ has been quantified and correlated to the network of ^{31}P nuclei more strongly dipolar coupled. This network is constituted by one ^{31}P nucleus and its 15 closest neighbors (within 4 Å), 11 in the same layer and 4 in the adjacent layer. Moreover the ^{31}P chemical shift tensors were experimentally and computationally determined, highlighting the existence of two kinds of magnetically non-equivalent phosphorus nuclei, differing for the orientation of the chemical shift principal axes frame.

This is the first study reporting a complete characterization of the nuclear spin interactions determining the ^{31}P NMR spectra of bP and of its exfoliated form fl-bP, which adds an important piece of information to the fundamental chemico-physical

knowledge of this “rediscovered” allotrope of phosphorus and supports increasing future applications of NMR to phosphorene-based materials.

ACKNOWLEDGMENT

The authors thank the European Research Council (ERC) under the European Union’s Horizon 2020 research and innovation program (grant agreement no. 670173) for funding the project PHOSFUN by an ERC Advanced Grant to M.P. Elisa Carignani is acknowledged for helpful discussion.

REFERENCES

-
- ¹ a) Novoselov, K. S.; Geim, A. K.; Morozov, S. V.; Jiang, D.; Zhang, Y.; Dubonos, S. V.; Grigorieva, I. V.; Firsov, A. A. Electric Field Effect in Atomically Thin Carbon Films. *Science* **2004**, *306*, 666-669. b) Novoselov, K. S.; Geim, A. K.; Morozov, S. V.; Jiang, D.; Katsnelson, M. I.; Grigorieva, I. V.; Dubonos, C. V.; Frisov, A. A. Two-dimensional Gas of Massless Dirac Fermions in Graphene. *Nature* **2005**, *438*, 197-200. c) Novoselov, K. S.; Jiang, Z.; Zhang, Y.; Morozov, S. V.; Stormer, H. L.; Zeitler, U.; Maan, J. C.; Boebinger, G. S.; Kim, P.; Geim, A. K. Room-Temperature Quantum Hall Effect in Graphene. *Science* **2007**, *315*, 1379.

² Lewis, E. A.; Brent, J. R.; Derby, B.; Haigh, S. J.; Lewis, D. J. Solution Processing of Two Dimensional Black Phosphorus. *Chem. Commun.* **2017**, 53, 1445-1458.

³ Hultgren, R.; Gingrich, N. S.; Warren, B. E. The Atomic Distribution in Red and Black Phosphorus and the Crystal Structure of Black Phosphorus. *J. Chem. Phys.* **1935**, 3, 351-355.

⁴ Brown, A.; Rundqvist, S. Refinement of the Crystal Structure of Black Phosphorus. *Acta Cryst.* **1965**, 19, 684-685.

⁵ Peruzzini, M.; Bini, R.; Bolognesi, M.; Caporali, M.; Ceppatelli, M. et al. A Perspective on Recent Advances in Phosphorene Functionalization and its Applications in Devices. *Eur. J. Inorg. Chem.* **2019**, 1476-1494.

⁶ Lei, W.; Liu, G.; Zhang, J.; Liu, M. Black Phosphorus Nanostructures: Recent Advances in Hybridization, Doping and Functionalization. *Chem. Soc. Rev.* **2017**, 46, 3492-3509.

⁷ Linga, X.; Wangb, H.; Huang, S.; Xiac, F.; Dresselhaus, M. S. The Renaissance of Black Phosphorus. *PNAS* **2015**, 112, 4523-4530.

⁸ Zhao, Y.; Chen, Y.; Zhang, Y.-H.; Liu S.-F. Recent Advance in Black Phosphorus: Properties and Applications. *Mater. Chem. Phys.* **2017**, 189, 215-229.

⁹ Passaglia, E.; Cicogna, F.; Costantino, F.; Coiai, S. et al. Polymer-Based Black Phosphorus (bP) Hybrid Materials by in Situ Radical Polymerization: An Effective Tool To Exfoliate bP and Stabilize bP Nanoflakes. *Chem. Mater.* **2018**, *30*, 2036-2048.

¹⁰ Caporali, M.; Serrano-Ruiz, M.; Telesio, F.; Heun, S.; Nicotra, G.; Spinella, C.; Peruzzini, M. Decoration of Exfoliated Black Phosphorus with Nickel Nanoparticles and its Application in Catalysis. *Chem. Commun.* **2017**, *53*, 10946-10949.

¹¹ Bolognesi, M.; Moschetto, S.; Trapani, M.; Prescimone, F.; Ferroni, C. et al. Noncovalent Functionalization of 2D Black Phosphorus with Fluorescent Boronic Derivatives of Pyrene for Surface Passivation and Band-Gap Tuning. *ACS Appl. Mater. Interfaces* **2019**, DOI: 10.1021/acsami.9b04344.

¹² Raucci, M. G.; Fasolino, I.; Caporali, M.; Serrano-Ruiz, M.; Soriente, A.; Peruzzini, M.; Ambrosio, L. Exfoliated Black Phosphorus Promotes in Vitro Bone Regeneration and Suppresses Osteosarcoma Progression through Cancer-Related Inflammation Inhibition. *ACS Appl. Mater. Interfaces* **2019**, *11*, 9333-9342.

¹³ Serrano-Ruiz, M.; Caporali, M.; Ienco, A.; Piazza, V.; Heun, S.; Peruzzini, M. The Role of Water in the Preparation and Stabilization of High-Quality Phosphorene Flakes. *Adv. Mater. Interfaces* **2016**, *3*, 1500441.

-
- ¹⁴ Lange, S.; Schmidt, P.; Nilges, T. Au₃SnP₇@Black Phosphorus: An Easy Access to Black Phosphorus. *Inorg. Chem.* **2007**, *46*, 4028-4035.
- ¹⁵ Mayo, M.; Griffith, K. J.; Pickard, C. J.; Morris, A. J. Ab Initio Study of Phosphorus Anodes for Lithium- and Sodium-Ion Batteries. *Chem. Mater.* **2016**, *28*, 2011-2021.
- ¹⁶ Wang, Y.; Yang, B.; Wan, B.; Xi, X.; Zeng, Z.; Liu, E.; Wu, G.; Liu, Z.; Wang, W. Degradation of Black Phosphorus: a Real-Time ³¹P NMR Study. *2D Mater.* **2016**, *3*, 035025.
- ¹⁷ Zhou, M.; Kim, S.; Mao, L.; Fujitsuka, M.; Zhang, J.; Wang, X.; Majima, T. Metal-Free Photocatalyst for H₂ Evolution in Visible to Near-Infrared Region: Black Phosphorus/Graphitic Carbon Nitride. *J. Am. Chem. Soc.* **2017**, *139*, 13234-13242.
- ¹⁸ Qiu, P.; Xu, C.; Zhou, N.; Jiang, F. Metal Free Black Phosphorus Nanosheets-Decorated Graphitic Carbon Nitride Nanosheets with C-P Bonds for Excellent Photocatalytic Nitrogen Fixation. *Appl. Catal. B-Environ.* **2018**, *221*, 27-35.
- ¹⁹ Hu, H.; Gao, H.; Gao, L.; Li, F.; Xu, N.; Long, X.; Hu, Y.; Jin, J.; Ma, J. Covalent Functionalization of Black Phosphorus Nanoflakes by Carbon Free Radicals for Durable Air and Water Stability. *Nanoscale* **2018**, *10*, 5834-5839.

²⁰ Wild, S.; Fickert, M.; Mitrovic, A.; Lloret, V.; Neiss, C.; Vidal-Moya, J. A.; Rivero-Crespo, M. A.; Leyva-Pérez, A.; Werbach, K.; Peterlik, H.; Grabau, M.; Wittkämper, H.; Papp, C.; Steinrück, H.-P.; Pichler, T.; Görling, A.; Hauke, F.; Abellán, G.; Hirsch, A. Lattice Opening upon Bulk Reductive Covalent Functionalization of Black Phosphorus. *Angew. Chem. Int. Ed.* **2019**, *58*, 5763-5768.

²¹ Ferrara, C.; Vigo, E.; Albin, B.; Galinetto, P.; Milanese, C.; Tealdi, C.; Quartarone, E.; Passerini, S.; Mustarelli P. Efficiency and Quality Issues in the Production of Black Phosphorus by Mechanochemical Synthesis: A Multi-Technique Approach. *ACS Appl. Energy Mater.* **2019**, *2*, 2794-2802.

²² Márkus, B. G.; Simon, F.; Nagy, K.; Fehér, T.; Wild, S.; Abellán, G.; Chacón-Torres, J. C.; Hirsch, A.; Hauke, F. Electronic and Magnetic Properties of Black Phosphorus. *Phys. Status Solidi B.* **2017**, *254*, 1700232.

²³ Plutnar, J.; Sofer, Z.; Pumera, M. Products of Degradation of Black Phosphorus in Protic Solvents. *ACS Nano* **2018**, *12*, 8390-8396.

²⁴ Filip, C.; Hafner, S.; Schnell, I.; Demco, D. E.; Spiess H.W. Solid State Nuclear Magnetic Resonance Spectra of Dipolar-Coupled Multi-Spin Systems under Fast Magic Angle Spinning. *J. Chem. Phys.* **1999**, *110*, 423-440.

²⁵ Schnell, I.; Spiess, H. W. High-Resolution ^1H NMR Spectroscopy in the Solid State: Very Fast Sample Rotation and Multiple-Quantum Coherences. *J. Magn. Reson.* **2001**, *151*, 153-227.

²⁶ Carravetta M.; Edén, M.; Zhao, X.; Brinkmann, A.; Levitt, M. H. Symmetry Principles for the Design of Radiofrequency Pulse Sequences in the Nuclear Magnetic Resonance of Rotating Solids. *Chem. Phys. Lett.* **2000**, *321*, 205-215.

²⁷ Martini, F.; Miah, H. K.; Iuga, D.; Geppi M.; Titman J. J. Measuring ^{19}F Shift Anisotropies and ^1H - ^{19}F Dipolar Interactions with Ultrafast MAS NMR. *J. Magn. Reson.* **2015**, *259*, 102-107.

²⁸ Hou, G.; Byeon, I.-J. L.; Ahn, J.; Gronenborn, A. M.; Polenova, T. Recoupling of Chemical Shift Anisotropy by R-Symmetry Sequences in Magic Angle Spinning NMR Spectroscopy. *J. Chem. Phys.* **2012**, *137*, 134201-134210.

²⁹ a) Haeberlen, U. In *Advances in Magnetic Resonance*; Suppl. 1; Waugh, J. S. Ed.; Academic Press: New York, 1976; b) Mehring, M. *Principles of High Resolution NMR in Solids*, 2nd. ed.; Springer Verlag: Berlin, 1983; c) Spiess, H. W. In *NMR Basic Principles and Progress*; P. Diehl, E. Fluck, R. Kosfeld, Eds.; Springer Verlag, Berlin, 1978, Vol. 15.

³⁰ Giannozzi, P.; Baroni, S. ; Bonini, N.; Calandra, M.; Car, R.; Cavazzoni, C.; Ceresoli, D.; Chiarotti, G. L. et al. QUANTUM ESPRESSO: a Modular and Open-Source Software Project for Quantum Simulations of Materials. *J. Phys.: Condens. Matter* **2009**, *21*, 395502.

³¹ Pickard, C. J.; Mauri F. All-Electron Magnetic Response with Pseudopotentials: NMR Chemical Shifts. *Phys. Rev. B* **2001**, *63*, 245101.

³² Latypov, S. K.; Polyancev, F. M.; Yakhvarov, D. G.; Sinyashin, O. G. Quantum Chemical Calculations of ³¹P NMR Chemical Shifts: Scopes and Limitations. *Phys. Chem. Chem. Phys.* **2015**, *17*, 6976-6987.